

November 1999
PSU/TH/221

Comparing classical and quantum probability distributions for an asymmetric infinite well

M. A. Doncheski ¹

Department of Physics

The Pennsylvania State University

Mont Alto, PA 17237 USA

and

R. W. Robinett ²

Department of Physics

The Pennsylvania State University

University Park, PA 16802 USA

Abstract

We compare the classical and quantum mechanical position-space probability densities for a particle in an asymmetric infinite well. In an idealized system with a discontinuous step in the middle of the well, the classical and quantum probability distributions agree fairly well, even for relatively small quantum numbers, except for anomalous cases which are due to the unphysical nature of the potential. We are able to derive upper and lower bounds on the differences between the quantum and classical results. We also qualitatively discuss the momentum-space probability densities for this system using intuitive ideas about how much time a classical particle spends in various parts of the well. This system provides an excellent example of a non-trivial, but tractable, quantum mechanical bound state problem where the correlations between the amplitude and curvature of quantum mechanical wavefunctions can be easily compared to classical intuition about particle motion, with quantitative success, but also warning of possible surprises in non-physical limiting cases.

¹mad10@psu.edu

²rick@phys.psu.edu

1. Introduction

The calculation of position-space energy eigenstates in quantum mechanical bound state systems is only the first step in student understanding of the underlying physics. Very often, a comparison of the resulting quantum probability densities, $|\psi(x)|^2$ versus x , with classical probability distributions provides much needed insight into the deep and pedagogically useful connections between the two approaches to mechanics. The most familiar problem of one-dimensional quantum theory, namely the infinite well, is, for example, occasionally discussed in this manner [1, 2]. The local averaging required to show that the oscillatory quantum probability distribution approaches the well-known flat classical value is easily implemented in this system, either visually or more analytically, to illustrate in detail the correspondence principle limit.

A far more familiar example and image in many modern physics and quantum mechanics texts is the comparison of the classical and quantum results for the harmonic oscillator eigenstates for increasingly large quantum number, appearing in both older classic texts [3, 4] and as well as in very recent ones [1, 2], [5] – [10] at a wide variety of levels. In this case, both the amplitude and the curvature (‘wiggleness’) of the wavefunction vary in a non-trivial and highly correlated way which can be understood using classical connections. A number of texts [1, 2], [6], [11] – [13] now emphasize the intuitive ideas behind the form of wavefunctions as dictated by the shape of the potential energy function and the value of the quantized energy eigenvalue, with examples including less familiar systems such as linear potentials [2, 8, 13, 14] and asymmetric infinite wells [2, 12, 13]. Similar comparisons are also possible for two-dimensional systems (such as the circular infinite well [15]) and an excellent discussion of the classical limit of the quantum solutions for the hydrogenic radial probability distributions has appeared in the pages of this journal [16].

Most such presentations can easily give the impression that the approach from the case of low-lying quantum states (small n) to the classical limit ($n \gg 1$) is smooth and uninteresting and in this note we wish to examine a simple system which exhibits some unexpected properties. The potential we consider is an asymmetric infinite well defined via

$$V(x) = \begin{cases} \infty & \text{for } x < -a \\ 0 & \text{for } -a < x < 0 \\ V_0 & \text{for } 0 < x < +b \\ \infty & \text{for } +b < x \end{cases} \quad (1)$$

so that it is an infinite well of width $(a+b)$, but with the right side at a higher (constant) value of potential. (In most of our numerical calculations, we will actually use values of $a = b$, but we will analyze the problem in some generality, at least initially.) Such a potential is shown in Fig. 1 (with specific values of a , b , and V_0 for later use.) This potential is useful for the discussion of semiclassical limits for several reasons:

- (i) It is a simple example where there is a non-trivial but easy-to-visualize variation of potential energy, and hence speed, between the classical turning points,
- (ii) the classical concepts of how much time a particle spends in each side of the well are intuitively obvious so that the classical probability distributions are straightforwardly obtained,
- (iii) the quantum solutions can be obtained in closed form, and the resulting energy eigenvalue conditions implemented numerically rather simply, and
- (iv) the Fourier transform of the position space solutions can be readily obtained to discuss the same qualitative and intuitive ideas in momentum space.

It is not surprising, perhaps, that several textbooks [7], [12], [13] use this system as a qualitative example of intuitive wavefunction analysis.

2. Quantum and Classical Solutions

To obtain the quantum solutions for this problem, we assume, at least initially, that $E > V_0$ (such as for those states labeled 5 and above in Fig. 1), and we solve the time-independent Schrödinger equation in each side of the well, obtaining solutions of the form

$$\psi(x) = \begin{cases} A \sin[k(x+a)] & \text{for } -a < x < 0 \\ B \sin[q(x-b)] & \text{for } 0 < x < +b \end{cases} \quad (2)$$

where

$$k = \sqrt{\frac{2mE}{\hbar^2}} \quad \text{and} \quad q = \sqrt{\frac{2m(E - V_0)}{\hbar^2}}. \quad (3)$$

These solutions already satisfy the boundary conditions at the two infinite walls. Insisting on the continuity of ψ and ψ' at the origin, the energy eigenvalue condition is given by

$$k \cos(ka) \sin(qb) + q \cos(qb) \sin(ka) = 0 \quad (4)$$

which is easily solved graphically and/or numerically. In the case where $E < V_0$, we can let

$$q = \sqrt{\frac{2m(E - V_0)}{\hbar^2}} = i\sqrt{\frac{2m(V_0 - E)}{\hbar^2}} = i\bar{q} \quad (5)$$

and use the same solutions and eigenvalue condition, but with the substitutions

$$\begin{aligned} \sin(qb) &\rightarrow \sin(i\bar{q}b) = i \sinh(\bar{q}b) \\ \cos(qb) &\rightarrow \cos(i\bar{q}b) = \cosh(\bar{q}b) \end{aligned} \quad (6)$$

and many multi-purpose mathematical packages such as *Mathematica*[®] can easily accommodate this change automatically. The energy eigenvalues can be generated for any given set of numerical parameters and the corresponding wavefunctions in (2) obtained and normalized.

For purposes of comparison with purely classical results, we note that the classical probability distribution for the particle when $E < V_0$ (where it would be restricted to bounce back and forth between the walls at $-a$ and 0) is

$$P_{CL}(x) = \begin{cases} 1/a & \text{for } -a < x < 0 \\ 0 & \text{for } 0 < x < +b \end{cases} . \quad (7)$$

This implies that the probability of finding the particle in the left side of the well in this case is

$$\text{Prob}[-a < x < 0] \equiv P_L^{(CL)} = 1 \quad \text{for } E < V_0. \quad (8)$$

For the case when $E > V_0$, the situation is more interesting and we can approach it by first calculating the time spent (classically) by the particle in the left (L) and right (R) sides of the well, namely

$$\begin{aligned} T_L &= 2a/v_L = 2a\sqrt{\frac{m}{2E}} \\ T_R &= 2b/v_R = 2b\sqrt{\frac{m}{2(E - V_0)}}. \end{aligned} \quad (9)$$

These combine to give the (classical) probability of finding the particle in the left side as

$$\begin{aligned} \text{Prob}[-a < x < 0] \equiv P_L^{(CL)} &= \frac{T_L}{T_L + T_R} = \frac{a/\sqrt{E}}{a/\sqrt{E} + b/\sqrt{E - V_0}} \\ &= \frac{a\sqrt{E - V_0}}{a\sqrt{E - V_0} + b\sqrt{E}} \\ &= \frac{a}{a + b\sqrt{E/(E - V_0)}} \end{aligned} \quad (10)$$

for $E > V_0$. (The final form is motivated by a discussion below.) In a similar way we find that

$$\text{Prob}[0 < x < +b] \equiv P_R^{(CL)} = \frac{b\sqrt{E}}{a\sqrt{E - V_0} + b\sqrt{E}}. \quad (11)$$

In the limit where $E \gg V_0$ (and the higher potential on one side has little effect) we have the purely geometric results

$$P_L^{(CL)} \longrightarrow \frac{a}{a+b} \quad \text{and} \quad P_R^{(CL)} \longrightarrow \frac{b}{a+b}. \quad (12)$$

Combining these results, we can evaluate the classical probability distribution for the general $E > V_0$ case, namely

$$P_{CL}(x) = \begin{cases} \sqrt{E - V_0}/(a\sqrt{E - V_0} + b\sqrt{E}) & \text{for } -a < x < 0 \\ \sqrt{E}/(a\sqrt{E - V_0} + b\sqrt{E}) & \text{for } 0 < x < +b \end{cases} \quad (13)$$

which is properly normalized since

$$\int_{-a}^{+b} P_{CL}(x) dx = 1. \quad (14)$$

In order to compare these classical quantities to the quantum results, we will eventually require the normalized, position-space energy eigenstates to evaluate

$$P_L^{(QM)} \equiv \int_{-a}^0 |\psi(x)|^2 dx \quad \text{and} \quad P_R^{(QM)} \equiv \int_0^{+b} |\psi(x)|^2 dx. \quad (15)$$

As an example of the possible solutions in such a system, we first choose a standard set of parameters, namely

$$\hbar = 2m = 1 \quad \text{and} \quad a = b = 3 \quad , \quad V_0 = 20 \quad (16)$$

and examine the results in detail, indicating below how general they are: specifically, we choose equal values of a and b to facilitate comparison between the quantum and classical probabilities of finding the particle in either side. With these parameters, the lowest 9 energy eigenvalues are given by

$$E_n = 0.95, 3.78, 8.44, 14.78, 20.84, 22.34, 24.94, 29.24, 33.30 \quad (17)$$

for $n = 1, \dots, 9$ and these are the values shown in Fig. 1 (as horizontal dashed lines) for the standard parameter set. (We note that the first four values, corresponding to

states mostly localized to the left side, have values which are appropriately smaller than the first four states for an infinite well of width a , namely $E_n^{(\infty)} = \hbar^2 \pi^2 n^2 / 2ma^2$; with this parameter set, for example, we find that $E_n/E_n^{(\infty)} \approx 0.85 < 1$ since the wavefunctions can penetrate into the classically disallowed region, thereby reducing their ‘wiggleness’ and kinetic energy.) We next plot, in Fig. 2, the normalized position-space probability densities, $|\psi(x)|^2$ versus x , for these states, using the appropriately normalized eigenfunctions. The vertical dashed line indicates the center of the well, while the solid horizontal lines (one only for the $E < V_0$ cases for 1 – 4, and two for the $E > V_0$ cases for 5 – 9) are the classical probability distributions in (7) and (13) respectively.

We first note the familiar general pattern of the addition of one ‘effective half wavelength’ or additional node as the quantum number increases, typical of all such bound state systems. For the 1 – 4 states, which are all below the V_0 threshold, the similarity to the corresponding infinite well results is clear, with the additional feature of the increased tunneling into the classically disallowed region. The first state above threshold, $n = 5$, is consistent with the usual intuitive rules about the behavior of wavefunctions in different potential regions. The wavefunction is wigglier (less wiggly) but with lower (higher) amplitude in the left (right) side where the classical kinetic energy and speed is larger (smaller) and the classical particle would be expected to spend less (more) time. The $n = 5$ state is even roughly consistent with the classical result (13), as far as such a low-lying state can be. Similar expected patterns (and qualitative agreement) are evident in the $n = 7$ and $n = 8$ states.

However, we note that the $n = 6$ wavefunction has an unexpected form, at least in terms of the relative values of the amplitudes on the left and right sides. In this case (as well as that for $n = 9$ where a similar effect is seen to occur) the wavefunctions being

matched at the (discontinuous) $x = 0$ boundary are connected (smoothly, of course) at what happens to be very close to an antinode. Since the amplitude in each side of the well is constant (since the potential is piecewise constant), if the wavefunctions match at an anti-node, the amplitudes must match ($A = B$ in (2)) everywhere in the well. Thus, while the ‘wiggleness’ of the wavefunction agrees with naive expectations based on considerations of classical speed and/or kinetic energy, the amplitudes and resulting probability densities are somewhat anomalous in that the particle will be found much more frequently (about half of the time in this case) in the left side of the well than expected from purely classical arguments. (Presumably, a student asked to sketch a possible solution in this potential well, as in Refs. [7, 12], and who provided something like this $n = 6$ case would not have received full credit!)

To discuss these effects more quantitatively, we calculate the quantum probability of finding the particle in the left-half of the well (15) for a number of states in this model system for comparison with the classical results given by (8) and (10). We plot, in Fig. 3, the quantum values (diamonds), $P_L^{(QM)}$, for all states with $E < 100$ (up to $n = 18$ in this case) for comparison to the solid curves representing the classical result. The horizontal dashed line indicates the high energy limit of $P_L = 0.5$ (when $a = b$) where the presence of a small potential ‘bump’ at the bottom of a very deep well (when $E \gg V_0$) will have little effect. We first note that for the states below threshold, the quantum probabilities, $P_L^{(QM)}$, decrease from near the purely classical value of $P_L^{(CL)} = 1$ due to the increasing amount of quantum tunneling evident in Fig. 1. Above threshold, the quantum probabilities seem to track the classical prediction (10), except most dramatically for the anomalous cases like $n = 6, 9$. In these instances, $P_L^{(QM)}$ is much larger than expected classically, but never exceeds $P_L = 0.5$ which would truly be unphysical as it would imply (classically) that the particle is moving slower in the

left side of the well and therefore spending more time there. A similar, but somewhat less dramatic, effect is also evident for those states with quantum probabilities which are significantly less than the classical predictions, such as the $n = 8$ state in Fig. 3. In all cases we have studied where P_L is most obviously much smaller than classical expectations, we have found that the wavefunction matching occurs very close to a node. The two extreme cases of anomalously large (small) values of $P_L^{(QM)}$ have thus been found to be connected to wavefunction matching near antinodes (nodes) at the discontinuous boundary.

Using this observation, we have been able to derive upper and lower bounds for $P_L^{(QM)}$ which we have found to be satisfied in all of our numerical studies. For example, in the case of matching at an antinode, the boundary condition on the left/right amplitudes (from the continuity of ψ) is $A = \pm B$ and the resulting quantum probabilities can be evaluated to find that

$$P_L^{(QM,max)} = \frac{a}{a+b} \quad (18)$$

which is also the high energy ($E \gg V_0$) limit. For the case of wavefunction matching at nodes, the appropriate condition comes from the continuity of ψ' , namely $kA = \pm qB$, which then gives

$$P_L^{(QM,min)} = \frac{a}{a+b[E/(E-V_0)]}. \quad (19)$$

(These results are considerably more simple in form than the general expression for $P_L^{(QM)}$ since we are integrating over integral numbers of half- and quarter-wavelengths in each side of the well in these special cases.) These two forms can be compared to the purely classical result (10) and we note that

$$\text{(node case)} \quad P_L^{(QM,min)} \leq P_L^{(CL)} \leq P_L^{(QM,max)} \quad \text{(antinode case)} \quad (20)$$

since $\sqrt{E/(E - V_0)} > 1$. To illustrate these bounds, we have plotted $P_L^{(QM,max)}$ (horizontal dashed line) and $P_L^{(QM,min)}$ (dotted curve) in Fig. 3 where they clearly bracket the classical result. We find that the results presented there are very typical of all the cases we have studied, namely that the quantum results for $P_L^{(QM)}$ rigorously fall between the upper and lower bounds, often coming very close to saturating them.

3. Quantum Results in a Smoothed Asymmetric Infinite Well

An obvious question about these effects (especially the anomalously large values of $P_L^{(QM)}$) is whether they are artifacts of the specific set of model parameters (16) used here or a more general phenomenon related to the structure of the potential well itself. We have repeated our analysis for a large number of different values of a, b , and V_0 (including many cases where $a \neq b$) and have almost always found that in the first 10-15 eigenstates above the V_0 threshold that there are 1-2 solutions which exhibit the wavefunction matching near antinodes which lead to anomalously large values of $P_L^{(QM)}$, compared to the classical result (10), almost saturating the upper bound (18), as well as 1-2 states which come close to saturating the lower bound (19). We think that it is easy to argue that these effects are a result of the discontinuous (and hence unphysical) nature of the potential step at $x = 0$. In order to test this, we have solved the Schrödinger equation for a ‘smoothed’ version of this asymmetric well given by

$$V_1(x) = \begin{cases} \infty & \text{for } x < -a \\ V_0/(1 + e^{-x/\delta}) & \text{for } -a < x < +b \\ \infty & \text{for } +b < x \end{cases} . \quad (21)$$

This version still has impenetrable walls at $x = -a, +b$, but gives a smoother transition between $V(-a) \approx 0$ and $V(+b) \approx V_0$ depending on the value of δ : the discontinuous step potential is recovered in the limit that $\delta \rightarrow 0$. This smoothed version is shown in Fig. 4 (middle) for $\delta = 0.2$ (as the dashed curve) along with the discontinuous

($\delta = 0.0$) step potential. We then solve the Schrödinger equation (numerically) to find the allowed energy eigenvalues and the resulting normalized eigenstates for the smoother case. The results for the $n = 6$ (top) and $n = 7$ (bottom) states are also shown in Fig. 4 where the wavefunctions for the $\delta = 0.2$ cases are shown (dashed curves) for comparison to the discontinuous case (solid curves.) For the anomalous $n = 6$ case, even the introduction of a small bit of ‘smoothness’ into the potential allows the wavefunction to accommodate to the required matching and the resulting quantum probability density is much closer to the classical expectation. On the other hand, for the $n = 7$ case, which was already in fairly good agreement with the classical result, the changes are much less dramatic. Similar smoothing functions yield similar results as we can see by considering a linear smoothing potential given by

$$V_2(x) = \begin{cases} 0 & \text{for } -a < x < -\epsilon \\ V_0(1 + x/\epsilon)/2 & \text{for } -\epsilon < x < +\epsilon \\ V_0 & \text{for } +\epsilon < x < +b \end{cases} . \quad (22)$$

If we expand both potentials (21) and (22) near the origin ($x \approx 0$) we find that they have a similar form, namely

$$V_1(x) \approx \frac{V_0}{2} \left(1 + \frac{x}{2\delta}\right) \longleftrightarrow \frac{V_0}{2} \left(1 + \frac{x}{\epsilon}\right) \approx V_2(x). \quad (23)$$

For numerical purposes, therefore, we will use $\epsilon = 2\delta$ for comparisons between the two smoothings. For example, in Fig. 4, we include the linear extrapolation (center) and the results for the $n = 6$ (top) and $n = 7$ (bottom) states as dotted curves (for $\epsilon = 0.4$). Not surprisingly, perhaps, the results are similar to the exponential smoothing.

In order to quantify the improvement in agreement with the classical results, we show in Fig. 5 the quantum probabilities, $P_L^{(QM)}$, for both the discontinuous ($\delta = \epsilon = 0.0$, diamond data as before) case and a smooth exponential ($\delta = 0.2$, starred data) case, compared again to the classical result (10). The agreement, in general, is much

better for the more physical potential gradient, except very near threshold (the $n = 5$ case) where small changes in the shape of the potential might be expected to have large results. We note that in each case (except for $n = 5$) that there is improvement (often substantial) in the agreement with the classical result.

At the same time, we show in Fig. 5 (top) the fractional change in the energy eigenvalue for the new smoothed potential compared to the discontinuous case, namely $\Delta E/E$, and note that while the energies are different by no more than 3% in the smoothed potential, the changes in the corresponding values of $P_L^{(QM)}$ are much more substantial, up to 100%. This implies that the introduction of the smooth (and hence more physical) potential step does not change the intrinsic properties of the system (energies, etc.) very much, but does allow for a more realistic description of the quantum probability densities and their approach to the classical limit. We find that in almost all cases where this type of anomalous behavior is encountered that the introduction of smoothing with a length scale $\delta \sim \epsilon \sim \lambda/4$ (where λ is the wavelength in the left side of the well) is enough to substantially improve agreement with the classical probability predictions while making little change in the energy eigenvalues.

4. Momentum Space Results

We can also develop our semi-classical intuition, as well as observing some of the anomalous quantum behavior, by examining the momentum-space probability densities for this system. The momentum-space wavefunctions, $\phi(p)$, can be obtained from the $\psi(x)$ in (2) using the Fourier transform via

$$\phi(p) = \frac{1}{\sqrt{2\pi\hbar}} \int_{-\infty}^{+\infty} \psi(x) e^{-ipx/\hbar} dx. \quad (24)$$

For the $\delta = 0.0$ case, where we can use the analytic results (2), the resulting normalized momentum-space probability distributions are easy to generate and we show them for

the same first 9 eigenvalues in Fig. 6. The vertical dashed lines correspond to the values of $p = \pm\hbar k$ (for all values of E) while the dotted lines indicate values of $p = \pm\hbar q$ (for states with $E > V_0$) where we would expect to see features corresponding to classical, back-and-forth motions in the left side ($p = \pm\hbar k$) and right sides ($p = \pm\hbar q$) of the well. For the states below threshold, the results are similar to familiar ones [2, 14] for the standard infinite well. For the $n = 5$ case, the first above threshold, we see a central feature, much like that for $n = 1$, as well as two small features at larger values of $|p|$. The similarity between the $E_1 = 0.95, k = 0.974$ central feature for $n = 1$ and the $E_5 - V_0 = 0.84, q = 0.914$ central peak for $n = 5$ is clear. The smaller features at larger values of $p = \pm\hbar k$ are qualitatively consistent with the small amount of time spent in the left-side of the well for this case where $q \ll k$. The anomalously large value of $P_L^{(QM)} \approx 0.5$ for the $n = 6$ case, where the particle spends roughly equal amounts of time in each side of the well, is evident in the approximately equal magnitudes of the q, k ‘bumps’ in this case. We note that in general we expect to see slightly larger (smaller) features at the smaller (larger) values of $p = \pm\hbar q$ ($p = \pm\hbar k$) due to our intuitive probability arguments ($P_R > P_L$) and this pattern is also reasonably evident for the $n = 7, 8$ cases. This pattern becomes increasingly difficult to identify, however, as n increases because the k, q features tend to merge due to the fact that

$$\begin{aligned}
k - q \propto \sqrt{E} - \sqrt{E - V_0} &= \sqrt{E} \left(1 - \sqrt{1 - \frac{V_0}{E}} \right) \\
&= \sqrt{E} \left(1 - 1 + \frac{V_0}{2E} + \dots \right) \\
&\approx \frac{V_0}{2\sqrt{E}}
\end{aligned} \tag{25}$$

which goes to zero as E increases. The difficulty with unambiguously identifying them is already evident in the $n = 9$ case where the classical k, q features are obvious, but the interference between the k, q terms gives rise to a feature between them which is even larger.

It is tempting to imagine trying to correlate, in a quantitative manner, the ‘amount of probability’ in the $\pm q$ and $\pm k$ ‘peaks’ with the position-space probabilities of measuring the particles in the right and left sides of the well respectively. We find, however, that given the large amount of interference between the k, q pieces of the Fourier transform necessary to obtain $\phi(p)$ that no such identification is possible.

5. Conclusions

In conclusion, we have identified a simple model quantum mechanical bound state system, the asymmetric infinite well, which can be easily analyzed and for which the comparison of the quantum and classical probability distributions finds many points of similarity, even exhibiting quantitative agreement for probabilities for many states. We have even been able to derive seemingly rigorous upper and lower bounds on how much the quantum results deviate from the classical probability expectations. The system can also be used to qualitatively examine classical intuition about momentum–space probabilities as well, given the relative simplicity of the position-space wavefunctions. However, it seems to yield, in almost every case studied, some solutions which have anomalous probability distributions, compared to classical expectations, due to the unphysical (discontinuous) nature of the potential. It also serves, therefore, as something of a cautionary tale about the use of idealized models.

Acknowledgments

The work of MAD was supported, in part, by the Commonwealth College of The Pennsylvania State University under a Research Development Grant (RDG); the work of RR was supported, in part, by NSF grant DUE-9950702.

References

- [1] Liboff R L 1997 *Introductory Quantum Mechanics* (Reading: Addison-Wesley) 3rd edition pp 95-99
- [2] Robinett R W 1997 *Quantum Mechanics: Classical Results, Modern Systems, and Visualized Examples* (New York: Oxford University Press) pp 115-120
- [3] Schiff L. I. 1949 *Quantum Mechanics* 1st Edition (New York: McGraw-Hill) pp 65-67
- [4] Sherwin C W 1960 *Introduction to Quantum Mechanics* (New York: Holt, Rinehart, and Winston) pp 52-53
- [5] Serway R A, Moses C J, and Moyer C A 1997 *Modern Physics* 2nd Edition (Fort Worth: Saunders) pp 210-211
- [6] Beiser A 1995 *Concepts of Modern Physics* (New York: McGraw-Hill) pp 188-189
- [7] Tipler P A and Llewellyn R A 1999 *Modern Physics* (New York: W. H. Freeman) pp 264-267
- [8] Goswami A 1992 *Quantum Mechanics* (Dubuque: Wm. C. Brown) pp 41-143
- [9] Griffiths D J 1995 *Introduction to Quantum Mechanics* (Englewood Cliffs: Prentice Hall) pp 41-43
- [10] Cohen-Tannoudji C, Diu B, and Laloë F 1977 *Quantum Mechanic* Volume I (New York: John Wiley) pp 501-502
- [11] Moore T A 1998 *Six Ideas That Shaped Physics Unit Q: Particles Behave Like Waves* (Boston: WCB/McGraw-Hill) pp 200-205, 219-226

- [12] Krane K S 1996 *Modern Physics* 2nd Edition (New York: John Wiley) p 172
- [13] Morrison M A 1990 *Understanding Quantum Physics: A User's Manual* (Englewood Cliffs: Prentice Hall) pp. 364-371, 377-379, 402-403
- [14] Robinett R W 1995 Quantum and classical probability distributions for position and momentum Am. J. Phys. **63** 823-832
- [15] Robinett R W 1996 Visualizing the solutions for the circular infinite well in quantum and classical mechanics Am. J. Phys. **64** 440-446
- [16] Rowe E G Peter 1987 The classical limit of quantum mechanical hydrogenic radial distributions Eur. J. Phys. **8** 81-87

Figure Captions

Fig. 1. Example of the asymmetric infinite well potential (1) for the special case of $a = b = 3$ and $V_0 = 20$. The nine lowest energy levels, obtained from the energy eigenvalue equation (4) with the parameters in (16), are shown as horizontal dashed lines.

Fig. 2. Normalized position-space probability densities, $|\psi(x)|^2$ versus x , for the first nine energy levels in the asymmetric well shown in Fig. 1 with the parameters in (16). The solid horizontal lines indicate the classical probability distributions (7) (for $E < V_0$ and states 1 – 4) and (13) (for $E > V_0$ and states 5 – 9). The vertical dashed lines indicate the center of the well at $x = 0$.

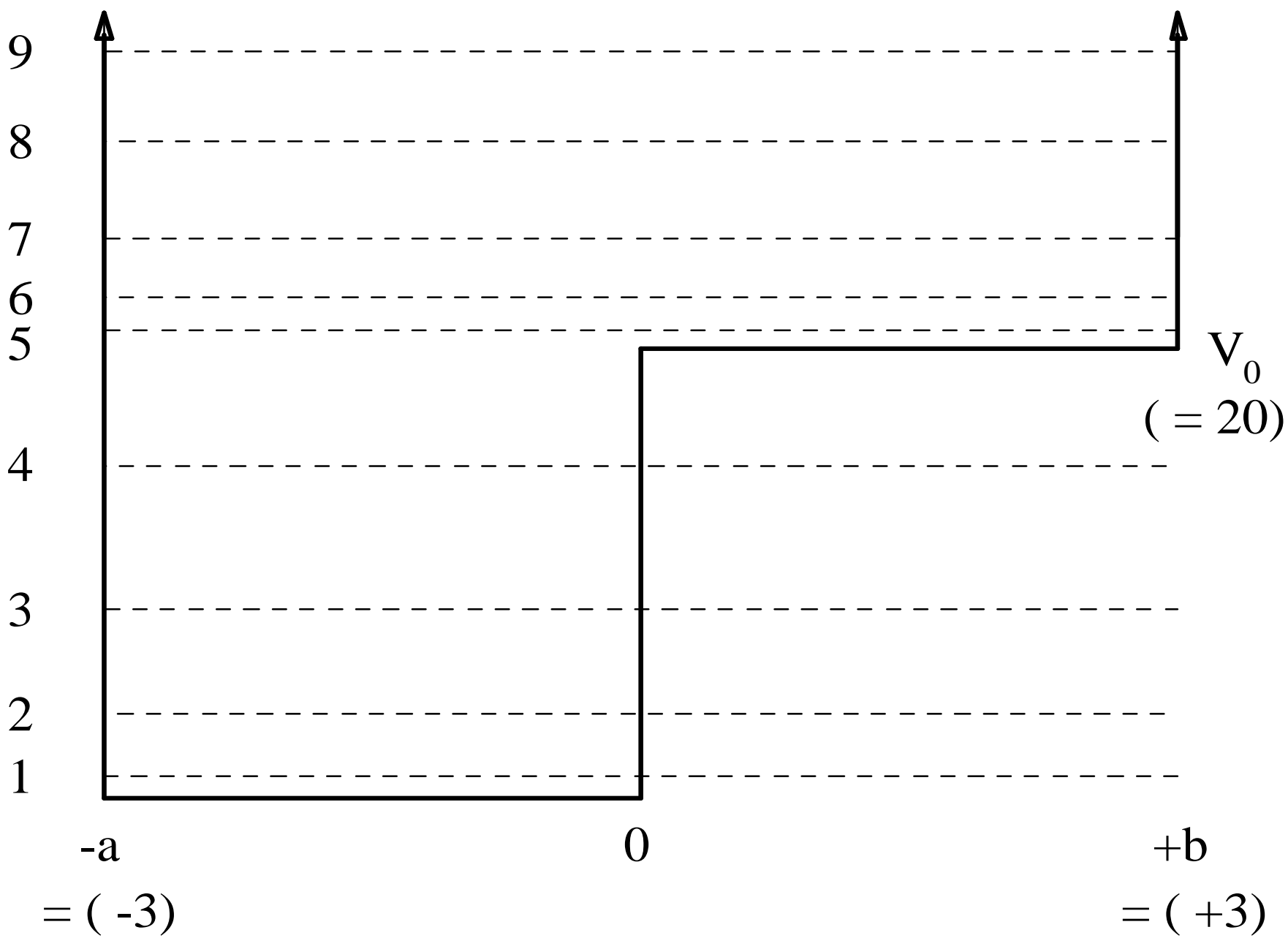
Fig. 3. Classical probability of finding the particle in the left side of the well (solid line and curve), given by (8) (for $E < V_0$ and states 1 – 4) and (10) (for $E > V_0$ and states 5 – 9), as a function of E for the states in Figs. 1 and 2 with the parameters in (16). The data points (diamonds) are the corresponding quantum probabilities, $P_L^{(QM)}$ (15), for the lowest 18 energy eigenvalues (all those with $E < 100$) with the standard parameter set. The horizontal dashed line at $P_L = 0.5$ corresponds to equal amounts of time spent in the left and right halves of the well which is also the upper bound (18), $P_L^{(QM,max)}$, for this case. The dotted curve is the corresponding lower bound (19), $P_L^{(QM,min)}$.

Fig. 4. The middle figure shows two ‘smoothed’ versions of the discontinuous step (solid curve) at the center of the well given by (21) ($\delta = 0.2$, dashed curve) and (22) ($\epsilon = 0.4$, dotted lines). The value of $\epsilon = 2\delta$ is chosen so that the two smoothings agree near $x \approx 0$ as in (23). The solutions corresponding to $n = 6$ (top) and

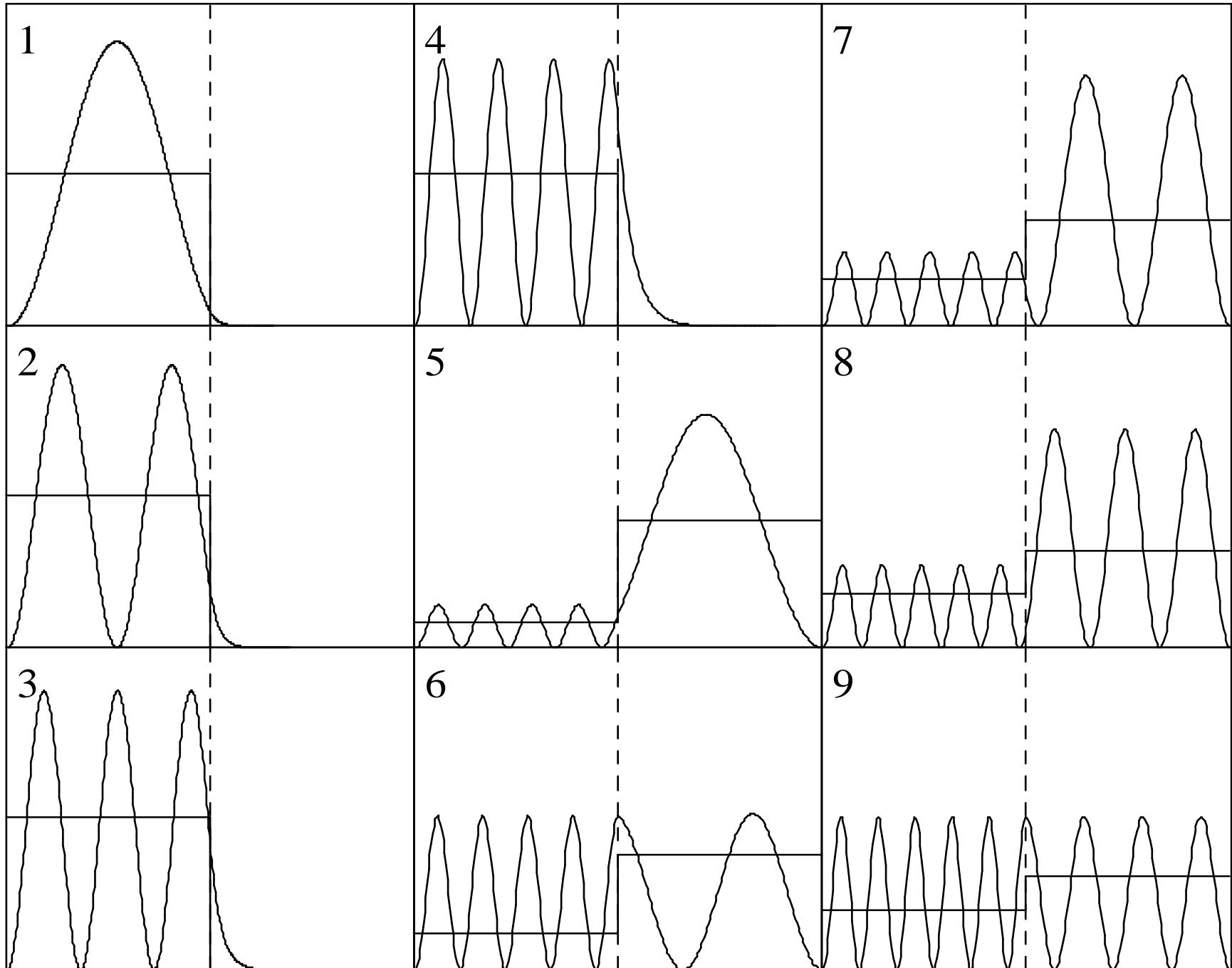
$n = 7$ (bottom) for the discontinuous well ($\delta = \epsilon = 0.0$, solid curves) and the smooth cases with $\delta = 0.2$ (dashed curves) in (21) and $\epsilon = 0.4$ (dotted curves) in (22) are shown. The ‘anomalous’ $n = 6$ case is affected dramatically and becomes much more consistent with the classical predictions for the smoothed cases, while the more standard $n = 7$ case is not affected very much.

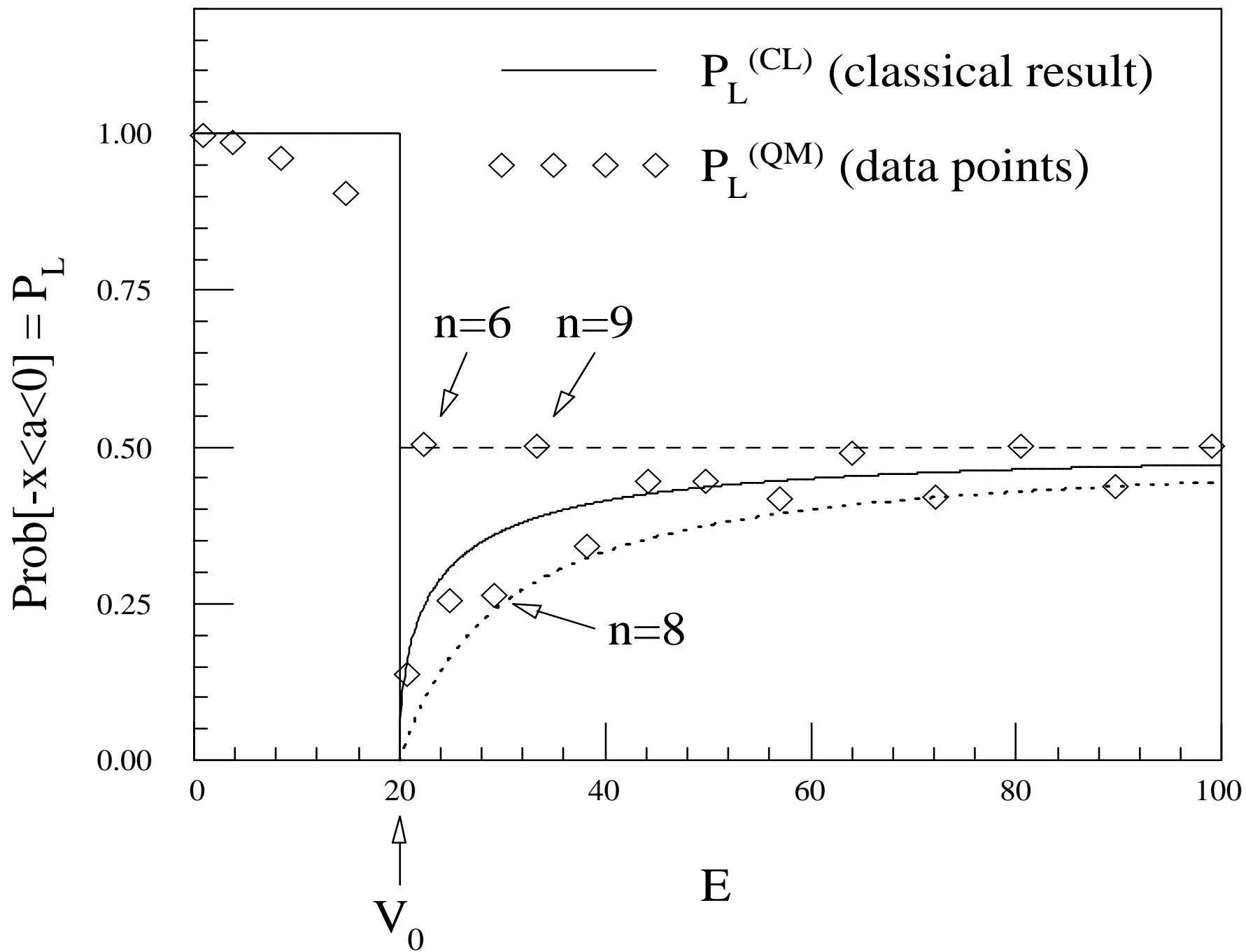
Fig. 5. Same as Fig. 3, but for $E > V_0$ only. The solid curve is the classical prediction for $P_L^{(CL)}$, and the results for the quantum probability from (15) for the discontinuous case ($\delta = 0.0$, diamonds again) and the smoothed case (21) with $\delta = 0.2$ (stars) are shown. The upper (dashed) and lower (dotted) bounds on $P_L^{(QM)}$ from (18) and (19) are indicated. Even a small amount of smoothing of the discontinuity improves the agreement with the expected classical result dramatically. The fractional change in energy $\Delta E/E$ induced for each state by using $\delta = 0.2$ compared to $\delta = 0.0$ is shown at the top. In no case is the change larger than 3% and it decreases quickly as the energy is increased.

Fig. 6. Normalized momentum-space probability distributions, $|\phi(p)|^2$ versus p , for the lowest nine states in the asymmetric well with the standard parameter set (16). The vertical dashed lines show values of $p = \pm\hbar k$ (for all E) and the dotted lines correspond to $p = \pm\hbar q$ (for $E > V_0$) from (3) for comparison. The momentum-space wavefunctions are calculated by taking the Fourier transform of the position-space solutions in (2).

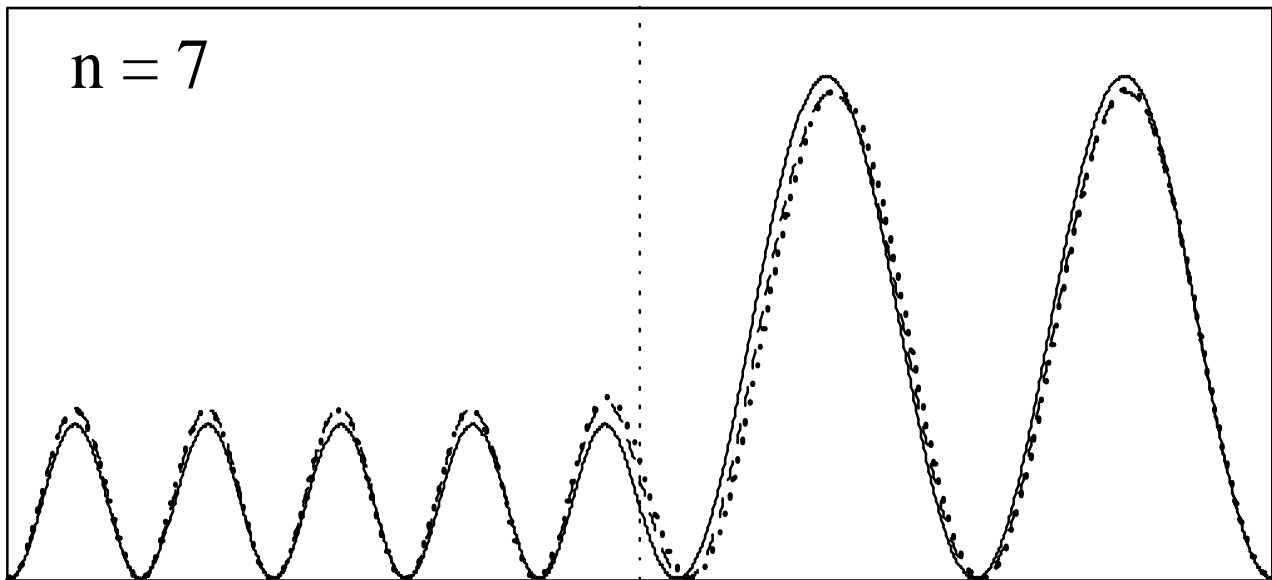
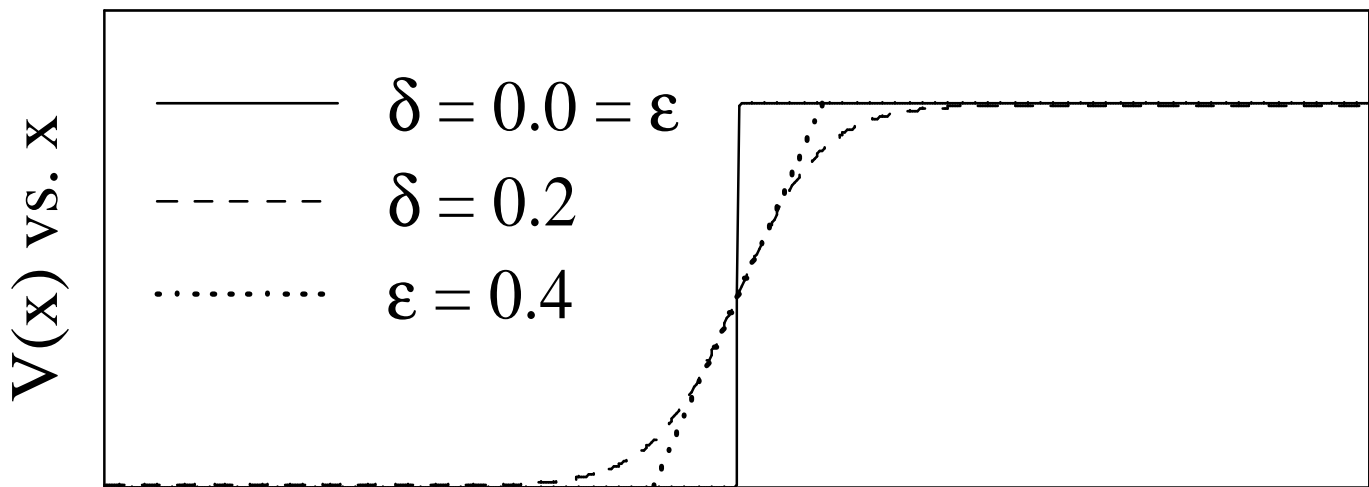
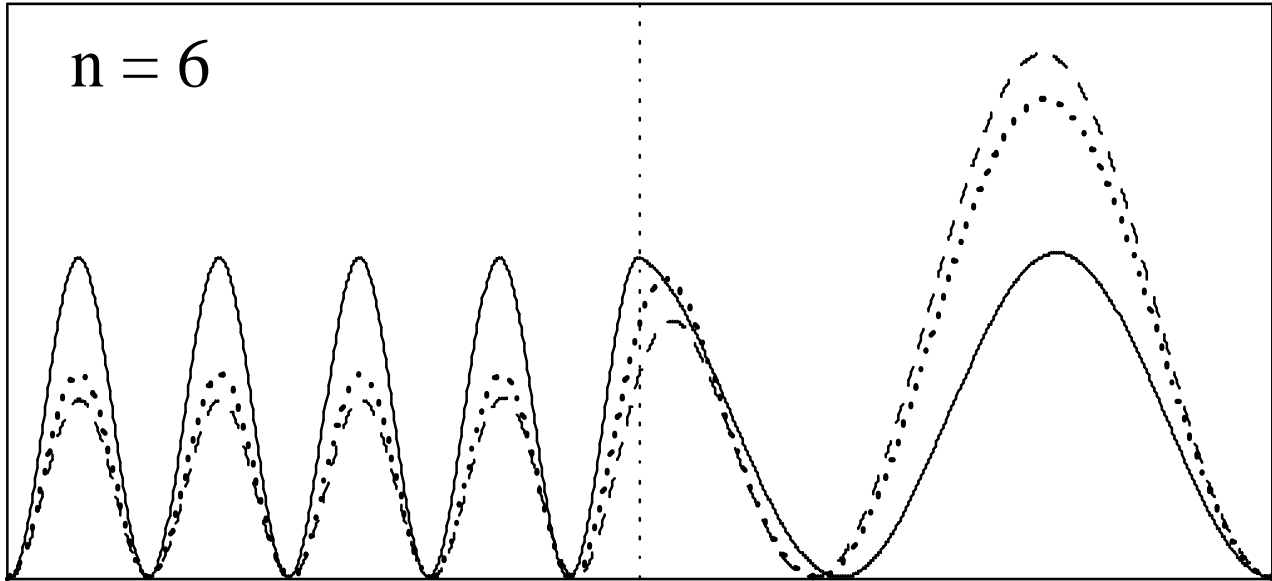


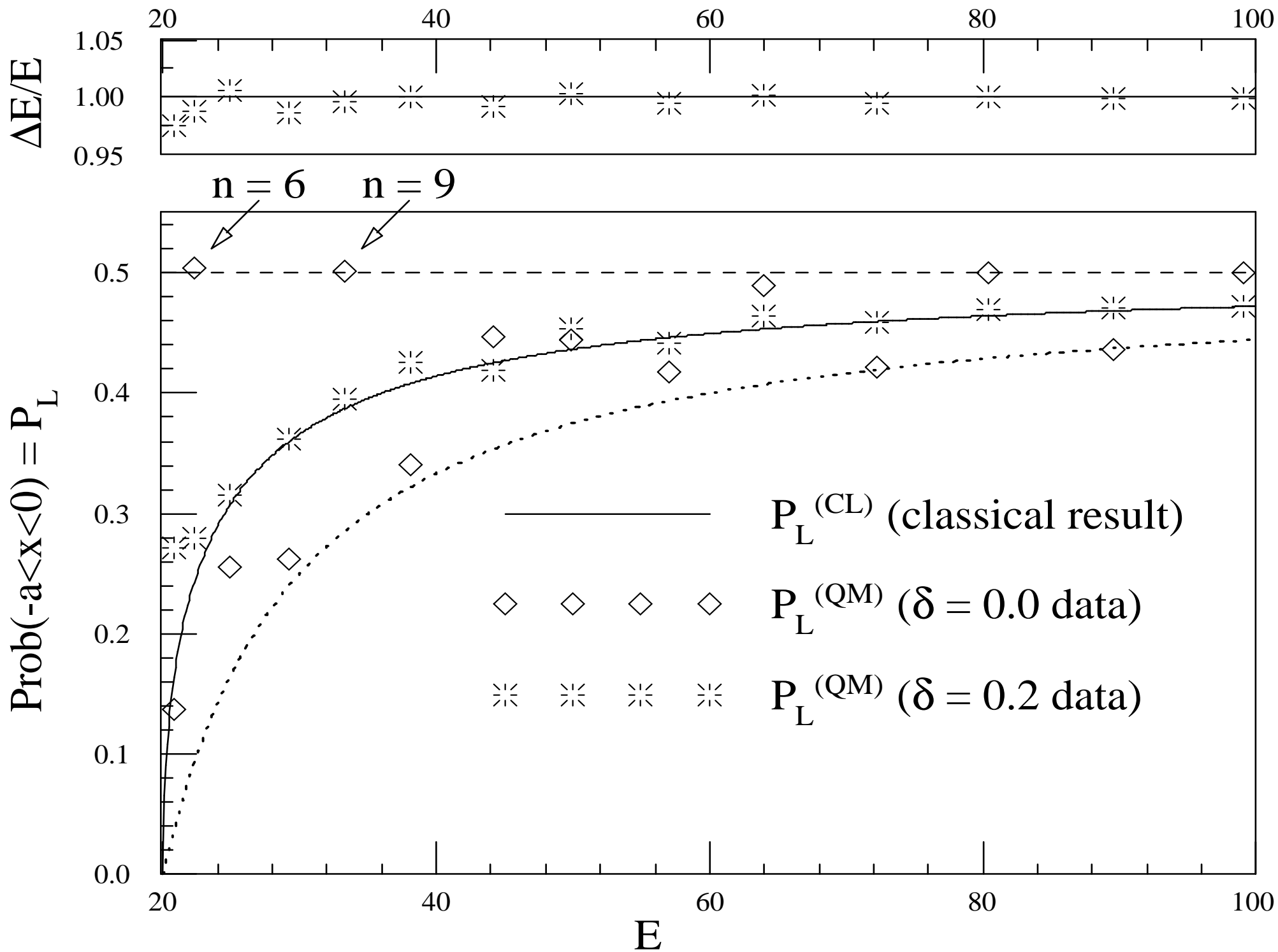
$|\psi(x)|^2$ vs. x





$|\psi(x)|^2$ vs. x





$|\phi(p)|^2$ vs. p

